Available online at www.sciencedirect.com
ScienceDirect
Biochemical and Biophysical Research Communications 357 (2007) 111–117
BBRC
www.elsevier.com/locate/ybbrc

Cell cycle-dependent mitochondrial biogenesis and dynamics in mammalian cells

Seungmin Lee [a,b,1], Sujeong Kim [a,b,1], Xuejun Sun [c], Jae-Ho Lee [a,b], Hyeseong Cho [a,b,*]

[a] Department of Biochemistry, Ajou University School of Medicine, Suwon, Republic of Korea
[b] Graduate School of Molecular Science and Technology, Ajou University, Suwon, Republic of Korea
[c] Department of Oncology, Cross Cancer Institute, Edmonton, Alta., Canada

Received 14 March 2007
Available online 26 March 2007

Abstract

During cell cycle progression and division, how cells coordinate mitochondrial biogenesis, distribution, and partitions remains to be clarified. Here, we show that mitochondrial mass and mitochondrial membrane potential increased from early G_1 to G_1/S and further gradually elevated to mitotic phase, indicating that mitochondrial biogenesis begins from early G_1 phase. In addition, mitochondrial DNA contents appeared to increase from G_1/S to G_2 phase during which a slight but consistent increase of NRF-1 level was observed. However, other transcriptional factors regulating mitochondrial biogenesis, mtTFA and PRC, were not changed. During interphase, heterogeneous mitochondrial population with different morphology and sizes were observed but reorganized into relatively homogeneous population of mitotic cells. Moreover, microtubule and dynein complex, $p150^{Glued}$ and dynein intermediate chain, strongly associate with mitochondria during interphase but dissociated from them during mitosis. Taken together, our results suggest that mitochondrial biogenesis and dynamics are tightly regulated during cell cycle progression.
© 2007 Elsevier Inc. All rights reserved.

Keywords: Mitochondrial biogenesis; Cell cycle; Microtubule; Dynein

Inheritance of eukaryotic cells not only includes genetic information but also cellular organelles. During the eukaryotic cell division cycle, cells have evolved a surveillance mechanism that ensures the accurate DNA replication and even partition of one copy of each chromosome into daughter cells [1]. Likewise, the number and size of any given organelle compartment should be properly regulated during cell division cycle [2–4]. How cells regulate organelle homeostasis during cell division becomes one of important issues in cell cycle.

Mitochondria are multitasking organelles involved in a number of cellular functions. They play central roles in the oxidative energy metabolism [5] as well as in apoptosis by integrating death signals [6,7]. Mitochondria exist in multiple copies in a cell and contain their own genomes. The number, morphology, and subcellular distribution of mitochondria can be dynamically altered during cellular growth and differentiation or when challenged with various cytotoxic conditions. The morphology and size of mitochondria can be controlled by mitochondrial fusion and fission events that are regulated by several proteins now being identified in yeast and mammalian cells [8–11]. Mitochondrial DNA (mtDNA) only provides 13 subunits of the oxidative phosphorylation enzymes in the respiratory chains of mitochondria and therefore, nuclear genes must provide the majority of components required for mitochondrial oxidative functions [12]. PGC-1α (peroxisome proliferator activated receptor gamma coactivator-1α) and PRC (PGC-1-related coactivator) have been identified as crucial factors linking external stimuli to mitochondrial biogenesis

* Corresponding author. Address: Department of Biochemistry, Ajou University School of Medicine, Suwon, Republic of Korea. Fax: +82 31 219 5059.
E-mail address: hscho@ajou.ac.kr (H. Cho).
[1] These authors contributed equally to this work.

0006-291X/$ - see front matter © 2007 Elsevier Inc. All rights reserved.
doi:10.1016/j.bbrc.2007.03.091

[13,14]. These coactivators interact with NRF-1 (nuclear respiratory factor 1) that trans-activates a number of nuclear genes involved in mitochondrial functions [15]. NRF-1 also mediates mtDNA transcription and replication through the mitochondrial transcription factor A (mtTFA). How all these different components involved in mitochondrial biogenesis and dynamics are regulated during cell cycle remained largely unknown.

In this study, we attempted to investigate how all these components related to mitochondrial biogenesis and dynamics coordinate during cell cycle progression.

Materials and methods

Reagents and antibody. MitoTracker Red (CMXRos), MitoTracker Green, 4′,6-diamidine-2-phenylindole (DAPI), and 10-nonylacridine orange (NAO) were obtained from Molecular Probes (Eugene, OR). The antibody against anti-dynein intermediate chain (DIC) antibodies was obtained from Sigma (Saint Louis, MO). Anti-voltage-dependent anion channel (VDAC) antibody was from Oncogene (Cambridge, MA).

Cell culture and cell synchronization. HeLa cells were grown in DMEM (Dulbecco's modified Eagle's Medium, Gibco-BRL, Grand Island, NY) supplemented with 10% FBS and maintained in CO_2 at 37 °C. Cells were synchronized at G_1/S boundary using the double thymidine block (DTB) method. For isolating cells in G_2 and mitotic phase, cells were treated with 100 ng/ml of nocodazole for 12 h and floating mitotic cells and residual adherent cells were separately collected. To obtain cells in early G_1 phase, the mitotic cells were allowed to further progress through G_1 phase for 4 h after complete removal of nocodazole.

FACS analysis. HeLa cells were synchronized at each phase and analyzed for DNA contents after propidium iodide staining by flow cytometry. To assess changes in mitochondrial mass and membrane potential, cells were incubated with 100 nM of MitoTracker Green, 1 μM of NAO or 125 nM of MitoTracker Red, for 30 min and washed with PBS. The stained cells were collected by trypsinization and the fluorescence intensities were measured by flow cytometry (FACS Vantage, Becton Dickinson).

RNA isolation and reverse transcription PCR. Total RNA was extracted using TRIzol reagent (Gibco-BRL) according to the manufacturer's instruction. To synthesize first-strand cDNA, 1 μg of RNA was reverse transcribed and the synthesized cDNAs were amplified in triplicate using specific primers. The primers used were: NRF-1 sense primer, 5′-GCA AAC GCA AAC ACA GGC C-3′; NRF-1 antisense primer, 5′-CTG CAT CTC CCT GAG AAG C-3′; PRC sense primer, 5′-GCA ACA GCC GTT CTG T-3′; PRC antisense primer, 5′-CTG CAA ATG CCT CCT C-3′; mtTFA sense primer, 5′-AAA AAG GAA AGC TAT GAC-3′; mtTFA antisense primer, 5′-AGC ACC ATA TTT TCG TTG-3′.

Total DNA isolation and real-time PCR. Cells were trypsinized, washed twice with PBS, and resuspended in 1× TE buffer. To break cell membrane, cells were frozen and thawed three times. Prepared DNA was analyzed by real-time PCR using ABI Prism 7000 Sequence Detection system (Applied Biosystems). Real-time PCR was performed according to the manufacturer's instruction. The primers used were: mtDNA primer, 5′-CACCCAAGAACAGGGTTTGT-3′; 18 S rDNA primer, 5′-TAG-AGGGACAAGTGGCGTTC-3′. The probe oligonucleotide sequences were: 6FAM-5′-TTACCGGGCTCTGCCATCT-3′-TAMRA for mtDNA detection and VIC-5′-AGCAATAACAGGTCTGTGATG-3′-TAMRA for 18 S rDNA detection. Real-time PCR amplification was performed in 1X TaqMan Universal PCR Master Mix (Applied Biosystems), using 100 nM primers and 200 nM probes. The thermal cycling conditions were 95 °C for 10 min, 50 cycles of 95 °C for 15 s and 60 °C for 1 min. Analysis of the data was performed using the ABI PRISM 7000 Sequence Detector Software to generate the individual standard curves from each experiment. A standard curve was rejected if the correlation coefficient of the trendline was <0.95.

Measurement of mitochondria and immunocytochemistry. To objectively resolve different lengths of mitochondria during cell cycle, mitochondria stained with 125 nM of MitoTracker Green and the images of mitochondria were captured using objective lenses (40X/NA1.3) under Two-Photon confocal microscopes (LSM510 NLO, Carl Zeiss). Lengths of mitochondria in living cells were determined in 3-dimensional confocal stacks with Imaris Software (Bitplane AG, Zurich, Switzerland). For immunocytochemistry, cells were stained for 30 min with 125 nM MitoTracker Red and fixed in a solution of methanol: acetone (1:1) for 10 min. Fixed cells were permeabilized for 5 min in PBS containing 0.075% Triton X-100, pre-incubated in blocking solution (1% bovine serum albumin in PBS), and then incubated overnight with appropriate primary antibodies at 4 °C. The cells were then washed, probed with a fluorescence-conjugated secondary antibody, and mounted for microscopic observation. All images were captured with a Confocal Laser Scanning Microscope (LSM510, Carl Zeiss).

Mitochondrial fractionation and immunoblotting. Cells were homogenized using Dounce homogenizer with Medium A (250 mM sucrose, 2 mM Hepes, pH 7.4, and 0.1 mM EGTA). Homogenate was centrifuged at 571*g* and the resultant supernatant was centrifuged at 14920*g* to get the mitochondrial fraction (pellet) and post-mitochcondrial fraction (supernatant). The mitochondrial and post-mitochondrial fractions were lysed with RIPA buffer. Proteins were run on polyacrylamide gels, transferred to nitrocellulose membrane, and immunoblotted with appropriate antibodies. The immunoblots were visualized by the enhanced chemiluminescence system (ECL, Amersham Pharmacia Biotech).

Results

Cell cycle-dependent increases of mitochondrial DNAs, mass, and membrane potentials

To investigate mitochondrial biogenesis during cell cycle progression, HeLa cells were synchronized at each phase of cell cycle (G_1/S, G_2, M, early G_1) using the double thymidine block (DTB) method and by nocodazole treatment. Analysis of the DNA contents by flow cytometry indicated that more than 90% of cells were arrested at mainly G_1 phase as well as at early S phases by the DTB synchronization (Fig. 1A). Releasing from the DTB allowed the cells to progress to G_2 and mitotic (M) phase; however, the authentic cell population of G_2 or M phase never reached 50% (data not shown). Alternatively, therefore, the cells in the G_2 phase (adherent cells) and at the M phase (floating cells) were separately collected after nocodazole treatment and flow cytometry analysis revealed that 70–90% of cells were arrested at G_2 and mitotic phase, respectively. Cell population at the sub-G_1 phase and $>4n$ is not indicated in the lower panel of Fig. 1A and the cells at G_2 phase were confirmed by cell cycle-dependent nuclear staining of CENP-F (data not shown). Synchronization of cells at the early G_1 phase (95%) was accomplished by allowing progression of the mitotic cells for 4 h. Each cell population at different phases was compared for the mitochondrial DNA (mtDNA) contents, mitochondrial mass as well as mitochondrial membrane potentials ($\Delta\psi_m$) per cell. In addition, we isolated total RNAs from each cell population and analyzed for the expression of transcription factors known to regulate mitochondrial biogenesis.

To investigate the changes in mtDNA during cell cycle progression, the nuclear 18 S ribosomal RNA gene (18 S

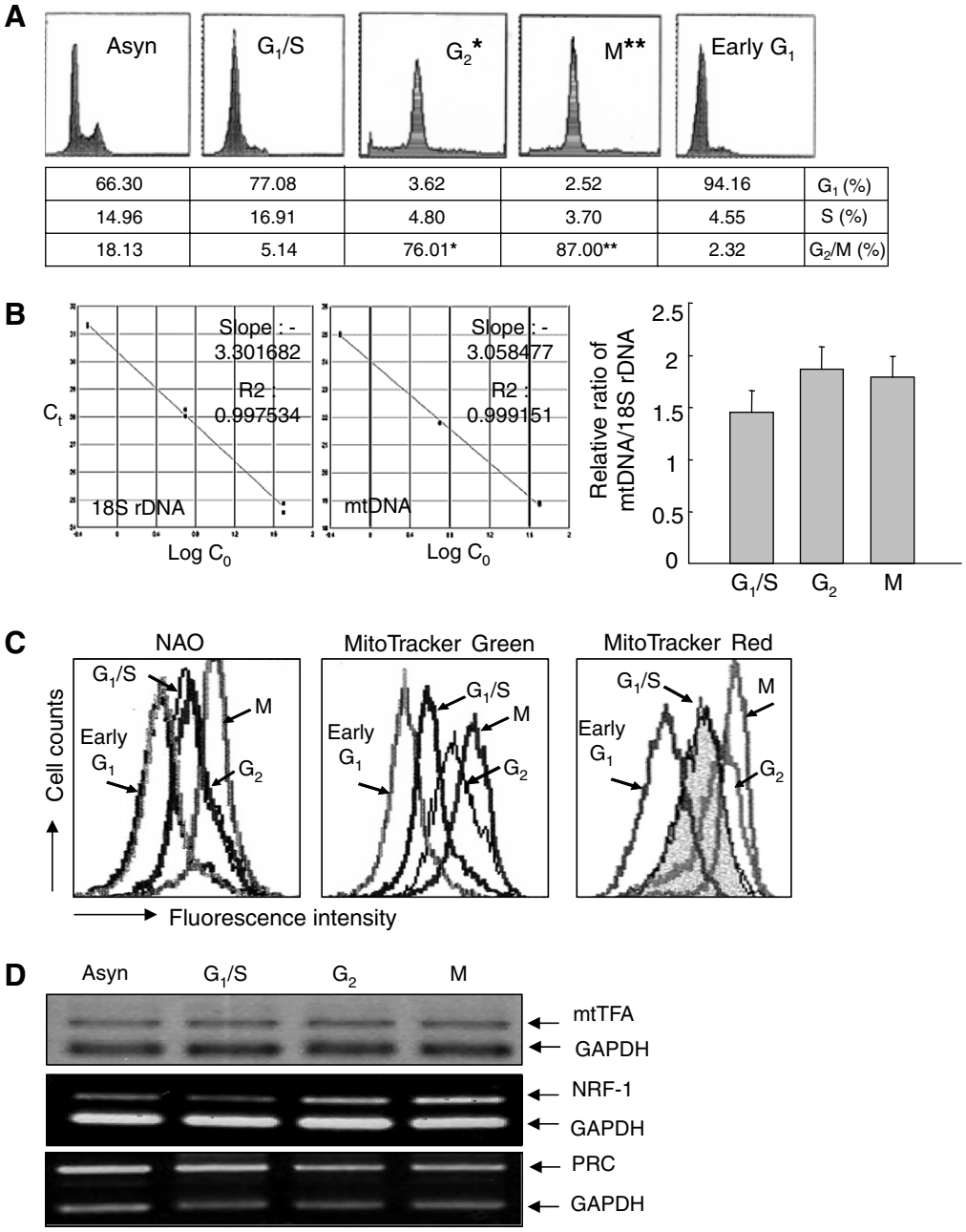

Fig. 1. Cell cycle-dependent changes of mitochondrial DNAs, mass, and membrane potentials. (A) HeLa cells were synchronized at each phase (G_1/S, G_2, M, early G_1) and analyzed for the DNA contents by flow cytometry. Cells at the G_2 (*) and M phases (**) were confirmed by anti-CENP-F and DAPI staining, respectively (data not shown). (B) Total DNAs were isolated from synchronized cells. The mtDNA contents were determined by real-time PCR using TaqMan probes. The DNA contents of mtDNA and 18 S rRNA gene (18 S rDNA) were calculated from the standard curve (left panel) and the relative ratios of mtDNA contents against 18 S rRNA gene were determined (right panel) in three independent experiments. Error bars represent the standard deviations. (C) The synchronized cells were stained with 1 μM of NAO, 100 nM of MitoTracker Green or 125 nM of MitoTracker Red, for 30 min before harvest. The fluorescence intensities were measured by flow cytometry. (D) Total RNA was isolated from synchronized cells and the mRNA levels of transcription factors were determined by RT-PCR.

rDNA) and mitochondrial DNA contents in each cell population were determined using fluorogenic probes and a real-time quantitative PCR system. The Ct value was determined using the software analysis by plotting the log of the changes in fluorescence intensities versus PCR cycle number of 10-fold serial dilution samples. The Sequence Detector Software (ABI PRISM 7000) generated each standard curve for 18 S rDNA and mtDNA (Fig. 1B, left panel) and the correlation coefficient of the trendline (R2) reaching >0.995 indicated relevance of quantification using this standard curve. Changes of the mtDNA contents through cell cycle progression were normalized to 18 S rDNA contents, presented as the relative ratios of mtDNA/18 S rDNA fluorescence intensities (Fig. 1B, right). We

observed that mtDNA contents increased consistently from G_1/S to G_2 phase in three independent experiments although the differences were not statistically significant.

We next explored the changes in mitochondrial mass and $\Delta\psi_m$ during cell cycle progression. We found that mitochondrial mass per cell increased from early G_1 to G_1/S and further gradually elevated until mitotic phase when measured by both fluorescent NAO probe indicating the accumulation of cardiolipin present in the inner mitochondrial membrane (Fig. 1C, left) and by MitoTracker Green probe (Fig. 1C, middle). Similarly, gradual increases of $\Delta\psi_m$ during cell cycle progression were also observed. Apparently, the mitochondrial mass and $\Delta\psi_m$ in mitotic cells reached the peak at mitotic phase then greatly reduced when these cells completed the cell division and entered into G_1 phase. Interestingly, the cells at the G_1/S boundary showed significantly higher mitochondrial mass and $\Delta\psi_m$ than those in early G_1 phase, indicating that mitochondrial biogenesis begins from early G_1 phase.

The biogenesis of mitochondria requires the expression of a large number of genes encoded by both nuclear and mitochondrial DNAs. NRF-1, mtTFA, and PRC are transcription factors that are known to be involved in mitochondrial biogenesis. We attempted to explore whether expression of these transcription factors changes during cell cycle progression using RT-PCR. Different sets of primers specific to these transcription factor genes were designed and the level of GAPDH mRNA was used as an internal control. When mRNA levels of these genes at different cell cycle phases were compared, we did not find any significant changes from mtTFA and PRC mRNA expression but consistently observed an increase of NRF-1 level from G_1/S phase to G_2 phase (Fig. 1D).

Cell cycle-dependent alteration of mitochondrial morphology

Cell cycle-dependent changes of mitochondrial morphology could be observed under time-lapse microscope. Like a very recent report by Martinez-Diez et al. [16], an intercon-

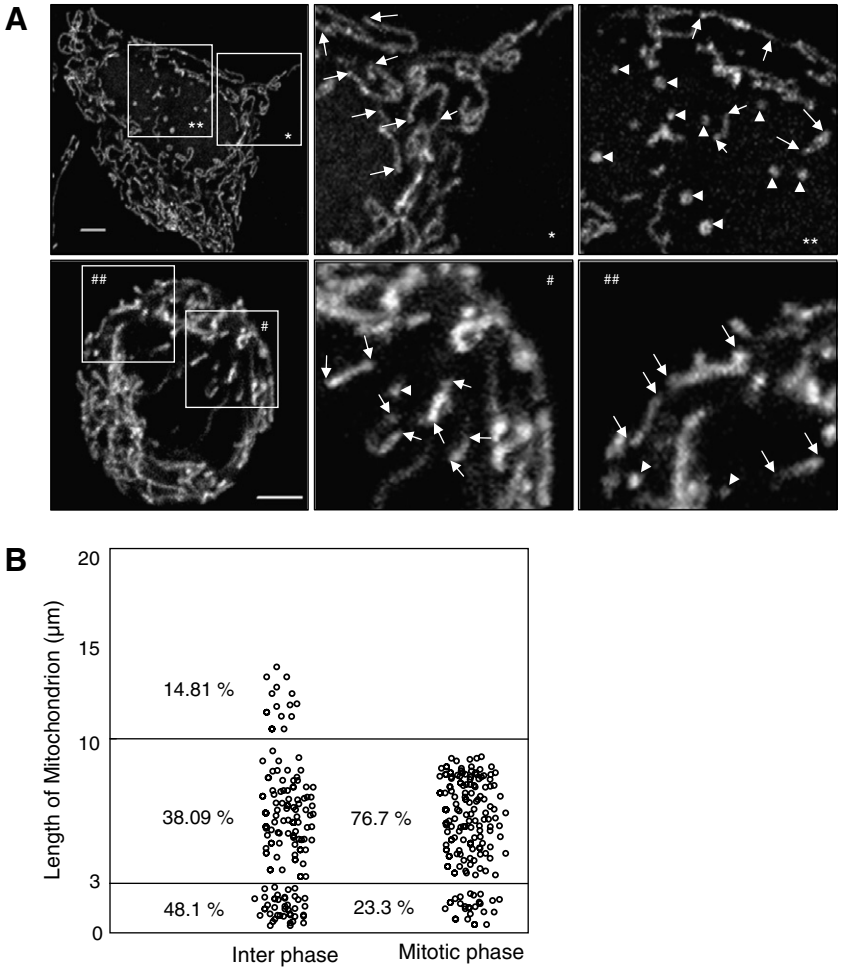

Fig. 2. Cell cycle-dependent reorganization of mitochondrial morphology. (A) To visualize mitochondria, cells in interphase (upper panel) and mitotic phase (lower panel) were stained with MitoTracker Green and images of mitochondria were captured under Two-photon confocal microscope. Arrowheads indicate small highly mobile mitochondria and two arrows indicate a single unit of mitochondria tubule. *, #: magnification on the right. Scale bars represent 5 μm. (B) The measurement was done on mitochondria which are either independent or can be identified as a single unit in a three-dimensional imaging using Imaris software program (Bitplane AG).

nected tubular network of mitochondria during interphase was found to be disintegrated at mitotic phase. In interphase cells, in fact, mitochondria were observed as highly interconnected tubular structures (data not shown) or long spiral forms of tubules (Fig. 2A, upper left and middle panels). We have also notified small highly mobile mitochondria (arrow heads) in interphase cells (Fig. 2A, upper right panel). On the other hand, in mitotic cells, an interconnected large tubular network of mitochondria was no longer visible but thickened and fragmented mitochondria of rather homogeneous lengths were predominant (Fig. 2A, lower panels). To objectively resolve different lengths of mitochondria during cell cycle, we measured lengths of mitochondria in living cells in 3-dimensional confocal stacks with Imaris Software (Bitplane AG, Zurich, Switzerland). In these measurements, interconnected tubular mitochondria in which ends of mitochondrial tubule were vague were excluded and approximately one hundred of mitochondria with visible distinct ends (Fig. 2A, two arrows for one mitochondrial tubule) were selected and measured. We found heterogeneous mitochondrial population from ones with relatively long spiral tubules (>10 μm) to ones with medium-sized tubules (3 μm < X < 10 μm) from interphase cells (Fig. 2B). In addition, highly mobile and small mitochondria (1–3 μm) were abundant in interphase cells. In mitotic cells, ~75% of them belonged to 3–8 μm, being much homogeneous in size. These results suggest that mitochondria in living cells undergo a series of fission and fusion events, especially before/after entering mitosis of cell cycle. Recently, many key molecules controlling mitochondrial fission and fusion events are discovered and it would be important to explore the functional role of these molecules during mitochondrial biogenesis.

Microtubule and dynein complex dissociate from mitochondria during mitosis

Mitochondria move along the cytoskeleton as a cargo of motor proteins [17] and therefore, the cytoskeleton plays a key role in determining different mitochondrial distributions and even function [18]. Consistent to the previous reports, we observed that localization of mitochondria in interphase cells showed a strong association with microtubules and displayed relatively weak association with actin (Fig. 3A). However, in mitotic cells, mitochondria no longer associated with microtubules and in fact, mitochondria were almost completely excluded from microtubules (Fig. 3B). In contrast, mitochondria of mitotic phase displayed rather a close association with actin but not with cytokeratin intermediate filament (Fig. 3B). It is known that microtubule-dependent transport of organelles occurs through the actions of two motor proteins, kinesin and dynein. Interestingly, we found that levels of $p150^{Glued}$ and dynein intermediate chain (DIC), major components of dynein motor complex, were drastically reduced in mitochondrial fraction of mitotic cells, indicating that the dynein complex is likely to detach from mitochondria during mitosis (Fig. 3B). Thus, our results strongly indicate that microtubules with dynein motors dissociate from mitochondria during mitotic phase.

Discussion

Despite relatively intensive studies on the molecular components of the mitochondrial fission and fusion machineries, researchers have not yet established how cell division cycle coordinates with mitochondrial biogenesis and dynamics. In the present study, we showed that mitochondrial mass and $\Delta\psi_m$ gradually increased from early G_1 to mitotic phase. Notably, when cells exit from mitotic phases and entered G_1 phase, all the fluorescence intensities of NAO, MitoTracker Green, and MitoTracker Red were drastically reduced, indicating that not only mitochondrial mass but also $\Delta\psi_m$ per cell were reduced after cell division. Recent report of Martinez-Diez et al. [16] partly supports our findings in that mitochondria mass increased significantly in the S phase but further increase of mitochondria mass at G_2/M phase was not observed. Since at least 75% of cells were synchronized at each phase of cell cycle in our experimental systems (Fig. 1A), cell cycle-dependent changes of mitochondrial mass at G_2 and M phases could be detectable. On the other hand, cell cycle-dependent increase of mtDNA was not as evident as of mitochondrial mass and $\Delta\psi_m$ but a consistent increase of mtDNA from G_1/S to G_2 phase was observed. Interestingly, increase of NRF-1 was also accompanied with increase of mtDNA at G_2 phase. It is shown that mtDNA synthesis occurred at multiple sites of the mitochondrial network and replication of mtDNA requires nuclear-encoded factors [19]. Thus, our findings here support their hypothesis that increased level of NRF-1 with mtTFA may coordinate mtDNA synthesis during cell division cycle.

Cell cycle-dependent morphological changes of mitochondria were first reported by Arakaki et al. [20]. We also showed that mitochondria exist as highly inter-connected tubular structures or long spiral forms of tubules during interphase but undergo a drastic reorganization upon mitotic entry. Importantly, it seemed that mitochondria not only underwent fragmentation but also had increased fusion events. Thus, mitochondria may reach a new set of equilibrium between fission and fusion events during mitosis. By measuring lengths of mitochondria in living cells, we found that mitochondria in interphase cells are highly heterogeneous. The lengths of mitochondria varied from the highly interconnected mitochondria network which cannot be measured by a simple length to highly mobile and spotty mitochondria (1–3 μm). However, in mitotic cells, majority of the mitochondria (~75%) are 3–8 μm in length, showing to be much more homogenous in length. Thus, it is likely that reorganization of mitochondrial morphology in mitotic cells includes a series of fission and fusion events before/after entering mitosis of cell cycle.

While the morphology of mitochondria is primarily controlled by fusion and fission events, the cytoskeleton can contribute to determining different mitochondrial

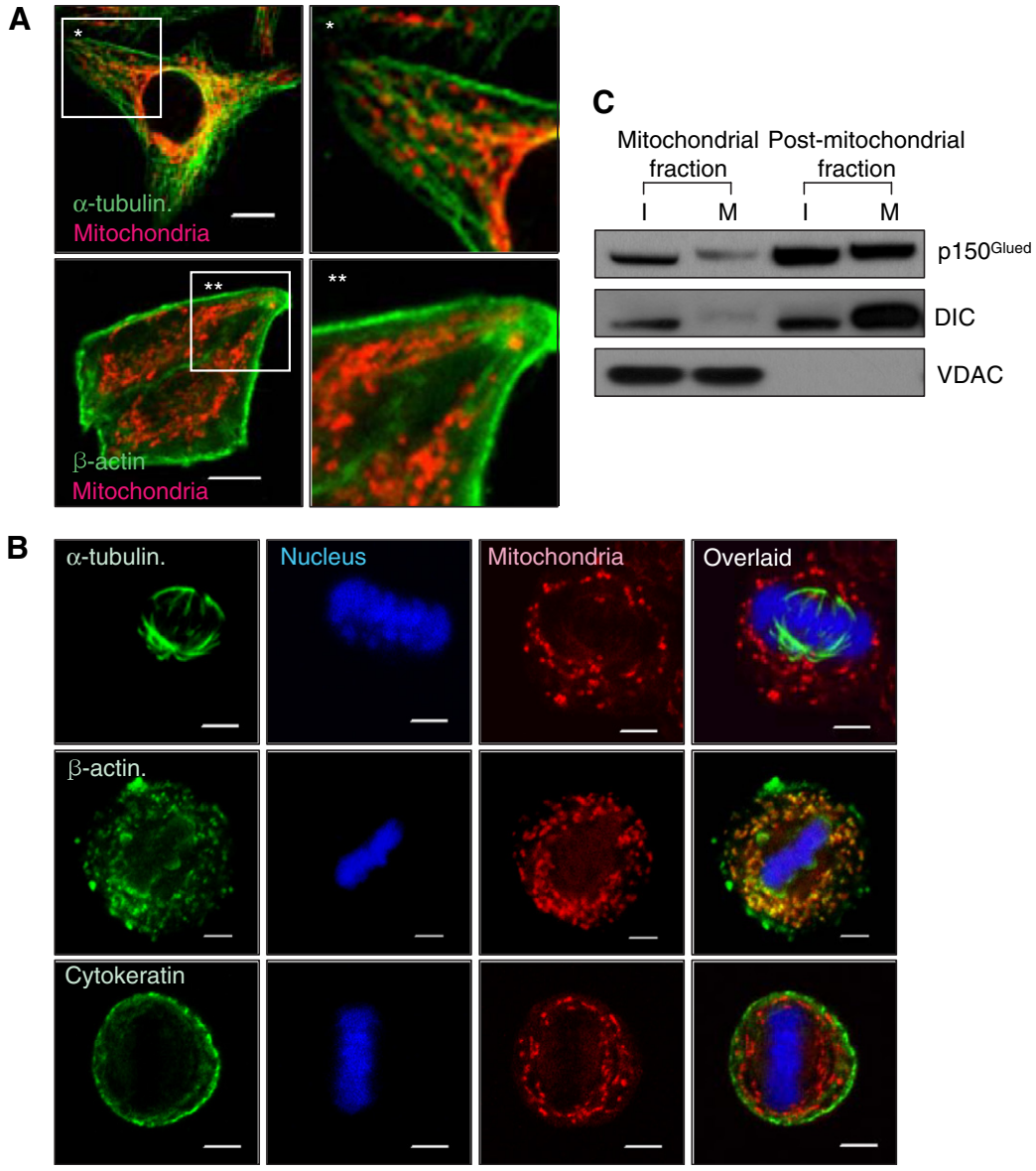

Fig. 3. Microtubule and dynein complex dissociate from mitochondria during mitosis. (A) Mitochondria (red) in interphase cells were co-visualized with microtubules (green, upper panel) or β-actin (green, lower panel) by immunofluorescence staining against α-tubulin or β-actin. * magnification on the right. Scale bars represent 10 μm. (B) Mitochondria (red) in interphase cells were co-visualized with microtubules, β-actin or cytokeratin. The condensed DNA was also visualized by DAPI staining. Scale bars represent 5 μm. (C) Mitochondrial and post-mitochondrial fractions were obtained from cells in interphase (I) and mitotic phase (M) after homogenizing cells using Dounce homogenizer and analyzed for the levels of $p150^{Glued}$ and dynein intermediate chain (DIC) by Western blotting. The VDAC expression is used to as a marker to indicate mitochondrial fraction.

morphology and distributions [21]. In fact, our results demonstrated that reorganization of mitochondria during mitosis was accompanied with detachment of microtubules and dynein motor complex from mitochondria. It is not known whether detachment of microtubules from mitochondria precedes or attributes to the mitochondrial reorganization. Notably, $p150^{Glued}$ and DIC bands in mitotic cells were up-shifted in both mitochondrial and post-mitochondrial fractions, indicating that these proteins undergo modification before/after mitotic entry. In fact, during xenopus oocyte maturation, $p150^{Glued}$ and DIC were found to be hyperphosphorylated by cdk1 kinase at early mitotic phase [22]. Similarly, cdk1 also could phosphorylate β-tubulin and this modification appeared to impair both GTP binding to β-tubulin as well as formation of tubulin dimers [23]. Thus, it would be interesting to see how cdk1 orchestrates reorganization of microtubule and mitochondria during G_2 to M transition in the future study. In summary, we here showed that cells tightly coordinate with mitochondrial biogenesis and dynamics during cell division cycle.

Acknowledgments

This study was supported by grants from the Korea Research Foundation (KRF 2006-312-E00040) and Korea

Science and Engineering Foundation through Chronic Inflammatory Disease Research Center (R13-2003-019).

References

[1] R. Visintin, E.S. Hwang, A. Amon, Cfi1 prevents premature exit from mitosis by anchoring Cdc14 phosphatase in the nucleolus, Nature 398 (1999) 818–823.
[2] S.V. Scott, A. Cassidy-Stone, S.L. Meeusen, J. Nunnari, Staying in aerobic shape: how the structural integrity of mitochondria and mitochondrial DNA is maintained, Curr. Opin. Cell Biol. 15 (2003) 482–488.
[3] J. Shorter, G. Warren, Golgi architecture and inheritance, Annu. Rev. Cell Dev. Biol. 18 (2002) 379–420.
[4] G. Warren, W. Wickner, Organelle inheritance, Cell 84 (1996) 395–400.
[5] M. Saraste, Oxidative phosphorylation at the fin de siecle, Science 283 (1999) 1488–1493.
[6] C. Brenner, G. Kroemer, Apoptosis. Mitochondria–the death signal integrators, Science. 289 (2000) 1150–1151.
[7] Y.J. Lee, S.Y. Jeong, M. Karbowski, C.L. Smith, R.J. Youle, Roles of the mammalian mitochondrial fission and fusion mediators Fis1, Drp1, and Opa1 in apoptosis, Mol. Biol. Cell 15 (2004) 5001–5011.
[8] J. Bereiter-Hahn, M. Voth, Dynamics of mitochondria in living cells: shape changes, dislocations, fusion, and fission of mitochondria, Microsc. Res. Tech. 27 (1994) 198–219.
[9] G.J. Hermann, J.W. Thatcher, J.P. Mills, K.G. Hales, M.T. Fuller, J. Nunnari, J.M. Shaw, Mitochondrial fusion in yeast requires the transmembrane GTPase Fzo1p, J. Cell Biol. 143 (1998) 359–373.
[10] R.E. Jensen, A.E. Hobbs, K.L. Cerveny, H. Sesaki, Yeast mitochondrial dynamics: fusion, division, segregation, and shape, Microsc. Res. Tech. 51 (2000) 573–583.
[11] D. Danino, J.E. Hinshaw, Dynamin family of mechanoenzymes, Curr. Opin. Cell Biol. 13 (2001) 454–460.
[12] R. Garesse, C.G. Vallejo, Animal mitochondrial biogenesis and function: a regulatory cross-talk between two genomes, Gene 263 (2001) 1–16.
[13] P. Puigserver, Z. Wu, C.W. Park, R. Graves, M. Wright, B.M. Spiegelman, A cold-inducible coactivator of nuclear receptors linked to adaptive thermogenesis, Cell 92 (1998) 829–839.
[14] R.C. Scarpulla, Nuclear control of respiratory gene expression in mammalian cells, J. Cell. Biochem. 97 (2006) 673–683.
[15] C.M. Chau, M.J. Evans, R.C. Scarpulla, Nuclear respiratory factor 1 activation sites in genes encoding the gamma-subunit of ATP synthase, eukaryotic initiation factor 2 alpha, and tyrosine aminotransferase. Specific interaction of purified NRF-1 with multiple target genes, J. Biol. Chem. 267 (1992) 6999–7006.
[16] M. Martinez-Diez, G. Santamaria, A.D. Ortega, J.M. Cuezva, Biogenesis and Dynamics of Mitochondria during the Cell Cycle: Significance of 3'UTRs, PLoS ONE 1 (2006) e107.
[17] S. Kim, H.Y. Kim, S. Lee, S.W. Kim, S. Sohn, K. Kim, H. Cho, Hepatitis B virus x protein induces perinuclear mitochondrial clustering in microtubule- and Dynein-dependent manners, J. Virol. 81 (2007) 1714–1726.
[18] V. Anesti, L. Scorrano, The relationship between mitochondrial shape and function and the cytoskeleton, Biochim. Biophys. Acta 1757 (2006) 692–699.
[19] J. Magnusson, M. Orth, P. Lestienne, J.W. Taanman, Replication of mitochondrial DNA occurs throughout the mitochondria of cultured human cells, Exp. Cell Res. 289 (2003) 133–142.
[20] N. Arakaki, T. Nishihama, H. Owaki, Y. Kuramoto, M. Suenaga, E. Miyoshi, Y. Emoto, H. Shibata, M. Shono, T. Higuti, Dynamics of mitochondria during the cell cycle, Biol. Pharm. Bull. 29 (2006) 1962–1965.
[21] K.J. De Vos, V.J. Allan, A.J. Grierson, M.P. Sheetz, Mitochondrial function and actin regulate dynamin-related protein 1-dependent mitochondrial fission, Curr. Biol. 15 (2005) 678–683.
[22] K.R. Dell, C.W. Turck, R.D. Vale, Mitotic phosphorylation of the dynein light intermediate chain is mediated by cdc2 kinase, Traffic (Copenhagen, Denmark) 1 (2000) 38–44.
[23] A. Fourest-Lieuvin, L. Peris, V. Gache, I. Garcia-Saez, C. Juillan-Binard, V. Lantez, D. Job, Microtubule regulation in mitosis: tubulin phosphorylation by the cyclin-dependent kinase Cdk1, Mol. Biol. Cell 17 (2006) 1041–1050.